Microfocus small-angle X-ray scattering at SSRF BL16B1 *

Wen-Qiang Hua(滑文强) Yu-Zhu Wang(王玉柱)[1)] Ping Zhou(周平) Tao Hu(胡涛)
Xiu-Hong Li(李秀宏) Feng-Gang Bian(边风刚) Jie Wang(王劼)

Shanghai Synchrotron Radiation Facility, Shanghai Institute of Applied Physics,
Chinese Academy of Sciences, Shanghai 201204, China

Abstract: Offering high-brilliance X-ray beams on micrometer length scales, the μSAXS at SSRF BL16B1 has been established with a KB mirror system for studying small sample volumes, or probing microscopic morphologies. The SAXS minimum q value is 0.1 nm^{-1} with a flux of 1.5×10^{10} photons/s. Two position-resolved scanning experimental methods, STXM and CT, are combined with μSAXS. To improve the significant smearing effect in the horizontal direction, an effective and easy-to-use desmearing procedure for two-dimensional SAXS patterns based on blind deconvolution was developed, and the deblurring results demonstrate the good restoration effect for the defocused image. Finally, a bamboo sample was used in the SAXS-CT experiment to illustrate the performance of the μSAXS method.

Keywords: small-angle X-ray scattering, KB mirror, smearing effects, image blind restoration

PACS: 41.50.+h, 61.05.cf **DOI:** 10.1088/1674-1137/41/4/048001

1 Introduction

The interaction of X-rays with inhomogeneities in matter can cause small deviations from their incident direction, called small-angle X-ray scattering (SAXS) [1]. As a non-invasive technique, SAXS is widely used to probe the micro/nano-scale structure and fluctuations of non-crystalline material, which are strongly related to system properties and functions [2]. The high photon flux and collimation provide by modern third-generation synchrotron sources has made SAXS a unique scattering technique in terms of angular and time resolution, small sample volume, etc. The third generation 3.5 GeV Shanghai Synchrotron Radiation Facility (SSRF) operates in top-up injection mode at a constant beam current of 240 mA [3]. Among the 7 Phase-I beamlines, BL16B1 is designed to satisfy the needs of a large variety of X-ray scattering experiments [4]. Owing to the excellent photon beam properties of the low-emittance source SSRF, BL16B1 has been optimized for performing in-situ time-resolved small/wide-angle X-ray scattering in both transmission and grazing-incidence geometries (time resolution of the order of sub-seconds). The community of SAXS facility users in China has grown rapidly in recent years [5]. However, SSRF users are not satisfied with the existing sub-millimeter beam size. An increasing quantity of research is performed with hierarchically structured nanocomposites, including polymer fibers, biological tissues, samples confined in micro-channels etc [6–8]. Given this, microfocus beam SAXS (μSAXS) is a suitable and powerful approach to study small scattering volumes. In addition, micro-structural variations in heterogenous samples can be mapped out by scanning sections with high precision. Furthermore, the μSAXS method has recently been combined with other scanning techniques, such as computed tomography (CT) and scanning transmission X-ray microscopy (STXM) [9, 10]. Many beamlines worldwide use μSAXS as a major technique, and a variety of optical focusing systems have been used to focus hard X-rays, including Kirkpatrick-Baez mirrors (KB mirrors), compound refractive lenses, Fresnel zone plates etc. At the European Synchrotron Radiation Facility, the ID13 beamline provides micrometer and sub-micrometer X-ray beams for in-situ time-resolved SAXS/wide-angle X-ray scattering applications [11]. The MiNaxs beamline of PETRA III was dedicated to micro/nano-focused X-ray scattering [12]. As a microfocus beamline in SSRF, BL15U1 was established for hard X-ray micro/nano-spectrochemical analysis, but with no plan to develop the μSAXS method, the limited sample-to-detector distance has become an obstacle [13]. Therefore, μSAXS was identified as a key technology urgently needed to probe small scattering volumes at BL16B1. The small source size and high flux in SSRF permit us to focus the beam to micrometer size using

Received 19 July 2016

∗ Supported by National Natural Science Foundation of China (11505278 and 11675253)

1) E-mail: wangyuzhu@sinap.ac.cn

highly demagnified optics, and obtain sufficient intensity to perform μSAXS. A new dedicated μSAXS station based on the BL16B1 was therefore proposed and constructed with a KB mirror system. In addition, the microfocus beam grazing incidence SAXS (μGISAXS) was also made available at the BL16B1. Furthermore, two position-resolved scanning experimental methods were developed for our users, SAXS-STXM and SAXS-CT. In this work, we particularly report an effective and easy-to-use desmearing procedure for two-dimensional SAXS patterns to improve the significant smearing effect in the horizontal direction. The SAXS-CT experimental results for a bamboo sample are presented to illustrate the performance of the μSAXS method.

2 Beamline optics and μSAXS experimental setup

2.1 Beamline optics

The photon source of the BL16B1 is introduced from a bend magnet of the SSRF. A schematic of the main optical components of the beamline is shown in Fig. 1 for the μSAXS method. Monochromatic hard X-rays of 5 to 20 keV are delivered by a Si(111) flat double-crystal monochromator (DCM) located 21 m from the source, and the energy resolution is $\Delta E/E = 4\times10^{-4}$@10 keV. A double focusing toroidal mirror is placed 4 m downstream from the DCM and used to focus the X-ray beam to the detector plane. A water-cooled white beam slit is placed 20 m from the source to define the incident beam's receiving angle (1.2 mrad×1 mrad). Since normal SAXS needs a well collimated and clean beam, three other monochromatic slits are situated at 23 m, 35 m and 38 m to collimate the downstream beam and suppress stray light from upstream.

To perform μSAXS experiments, a micro-sized hard X-ray beam is necessary for small volume scattering analysis, while a small beam divergence after the sample will keep the SAXS pattern away from the smearing effect. In theory the signal-to-noise ratio of SAXS experiments stands to benefit from the high photon density of the incident hard X-ray beam. Many types of focusing elements are available for μSAXS beamlines. Considering their wide energy range, low flux loss and convenience of adjustment, KB mirrors are a good choice for the μSAXS system at SSRF BL16B1. Thus, when in μSAXS mode, a KB mirror system is installed 38.5 m from the source (see the top-right corner of Fig. 1). At an energy of 10 keV, a focused X-ray spot was achieved at the sample position with a flux of 1.5 × 10^{10} photons/s, with a beam size of 19.9(±0.1) μm (horizontal) × 13.5(±0.1) μm (vertical) ((see the bottom-left corner of Fig. 1)) and a divergence of about 1.76(±0.05) mrad (horizontal) × 0.55(±0.05) mrad (vertical). The calculated average photon density of the focused X-ray beam was about 5.6 × 10^{7} photons/s/mm^2, which is 474 times greater than that of normal SAXS (flux: 1.5 × 10^{11} photons/s; beam size: 1600 μm× 800 μm; calculated average photon density: 1.2 × 10^{5} photons/s/mm^2). To get a clean incident beam and low background data, an anti-scattering pinhole was placed upstream from the sample. As a

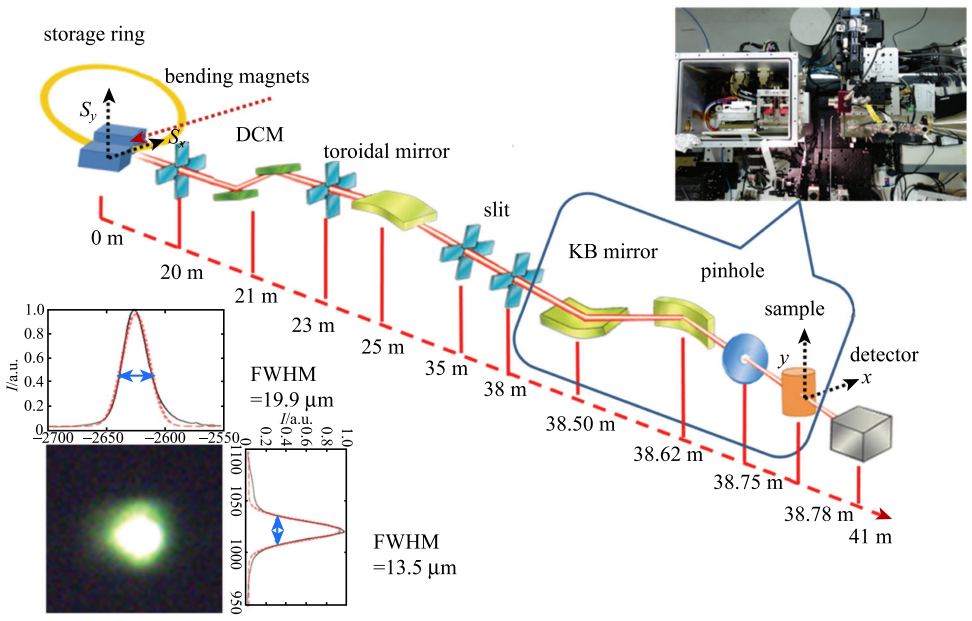

Fig. 1. Schematic diagram of beamline BL16B1 for the μSAXS method at SSRF.

conventional piece of equipment for the SAXS endstation, a 2 m evacuated flight tube (sealed by kapton windows) was placed between the sample and the detector to reduce additional signal due to air scattering. The two-dimensional (2D) SAXS data were recorded using a Mar165 CCD or a Pilatus 200K(DECTRIS) detector. In order to protect the detector from radiation damage from the direct beam, several beam-stops of different sizes and shapes (circular and rectangular) are available. In addition, there are two beam intensity monitors including a N_2 gas ionization chamber before the sample and a photodiode in the beam stop after the sample.

2.2 μSAXS experimental modes and data acquisition

SAXS is an averaging technique that accesses nano-scale structures but cannot spatially resolve extended samples. Standard x-ray absorption CT has been used for many years for non-invasive 3D studies, and provides access to volume-resolved information. While providing excellent spatial resolving power, it has an inherent lack of information about the nano-scale structure of the sample [10]. High-resolution scanning techniques like STXM reveal information that is typically limited to covering small fields of view in the micrometer range to very thin samples. Full-field two-dimensional X-ray microscopy reveals invaluable information but not down to the nano-scale. [9]. Hence, a combination of SAXS and STXM (or CT) sensitive to nano-scale structures averaged over a spatial area in the square-micron range is suitable for imaging samples of several millimeters to centimeters. The set-up for both SAXS-CT and SAXS-STXM measurements at the BL16B1 are depicted in Fig. 2. For the SAXS-STXM measurements, the incident monochromatic X-ray beam was focused to about 19.9 μm × 13.5 μm at the sample position for the raster scan measurements. To speed up data acquisition, scattering was recorded in a continuous line scan mode with the sample moving along a line of the 2D raster scan while the 2D detector was recording data accordingly. Similarly, for the SAXS-CT measurements, 2D SAXS patterns were collected point by point for each horizontal sample translation s, and rotation ω. In addition,

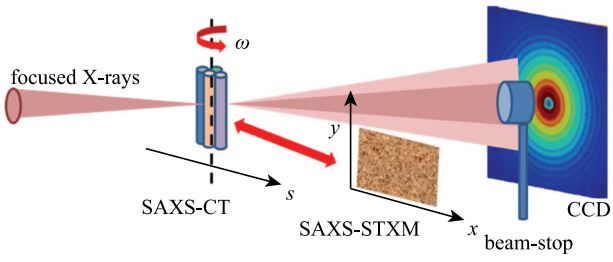

Fig. 2. (color online) Experimental set-up for both SAXS-CT and SAXS-STXM measurements.

one-dimensional scanning μGISAXS has also been developed for our users. All these experimental methods open up a vast field of applications in the investigations of the distribution and orientation of nano-scale structures over extended areas.

3 Preliminary experiment and data desmearing

The two-dimensional μSAXS patterns of a widely used standard sample, bull collagen fiber, were recorded at BL16B1 of SSRF, with the sample placed horizontally and vertically as shown in Fig. 3(a, b). These intensity profiles were transformed into normalized logarithmic distributions and good signal-to-noise ratio could be achieved with 100 seconds of exposure time. The SAXS resolution was imposed by the beamstop size and the minimum $q = 2\pi/\lambda \sin 2\theta = 0.1(\pm 0.01)$ nm^{-1}can be obtained in the vertical direction at the energy of 10 keV X-rays, as shown in Fig. 3(c). However, the direct beam profile was about 3.5(±0.1)mm × 1.1(±0.1) mm, as shown in Fig. 3(d). Because of the smearing effect of the direct beam profile in the horizontal direction, the bandwidth of the SAXS streaks was broadened markedly, which will lead to uncertainty in the peak width and position.

Instrumental smearing effects, originating from limitations in instrument resolution, can in many instances lead to errors in the SAXS data analysis, or, if data are severely smeared, they can prevent quantitative analysis altogether [14]. With SAXS at modern synchrotron radiation facilities, the smearing effect is usually disregarded because the approximation of an ideal pencil beam is frequently sufficient for the quantitative data analysis. This may not be appropriate, however, for tabletop SAXS and μSAXS set-ups [14, 15]. In this case, desmearing of the μSAXS data to correct for instrumental resolution is necessary.

3.1 Analysis of the smearing effect in μSAXS data

The main source of SAXS instrumental smearing originates from finite collimation (the beam profile or divergence), finite detector resolution (pixel size), wavelength spread, beam profile at the sample and finite sample thickness [1, 16]. All these aspects contribute to a smearing or blurring effect on the observed scattering pattern, and the definition or sharpness of the SAXS pattern can be reduced, which may lead to a misestimate of the regularity of arrangement in the material. A number of studies have been performed in order to investigate the smearing effect in SAXS experiments. The true scattering cross section $I_{\rm ideal}(q)$ yields the smeared intensity $I_{\rm obs}(q)$, through a convolution with the

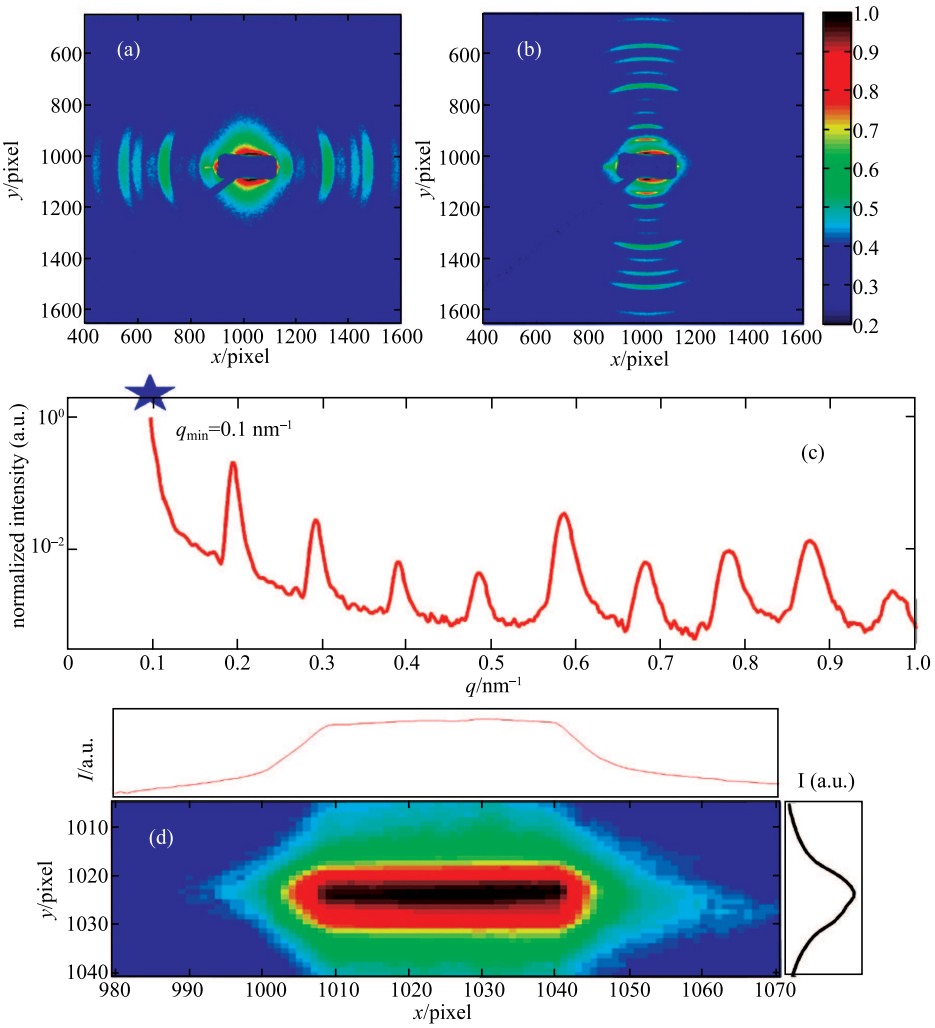

Fig. 3. (color online) The μSAXS pattern of a horizontally (a) and vertically (b) placed bull collagen fiber sample measured at BL16B1 of SSRF; (c) Normalized azimuthal integrated intensity distribution in logarithmic scale marked with $q_{\min}$ for (b); (d) The direct beam profile recorded by a detector with aluminum attenuator.

resolution function or point-spread function (PSF) $R(q,q')$,

$$I_{\rm obs}=\int_{q'}R(q,q')I_{\rm ideal}(q')\,{\rm d}q'+n(q), \tag{1}$$

where $n(q)$ is the noise introduced in the procedure of image acquisition. An analytical treatment of the resolution functions describes the contributions of different Gaussian functions. For a finite wavelength spread of the radiation, the full width at half-maximum (FWHM) of the Gaussian resolution function is

$$\sigma_\lambda(q')=\frac{1}{2(2\ln 2)^{1/2}}\frac{\Delta\lambda}{\lambda}q'. \tag{2}$$

Besides, the geometric factor $\sigma_{\rm geo}$ also contributes to the total resolution parameter $\sigma_{\rm tot}$,

$$\sigma^2_{\rm tot}(q')=\sigma^2_\lambda(q')+\sigma^2_{\rm geo}, \tag{3}$$

where the geometric contribution includes the finite collimation $\sigma_{\rm C}$ and the detector resolution $\sigma_{\rm D}$: $\sigma^2_{\rm geo}=\sigma^2_{\rm C}+\sigma^2_{\rm D}$ [16].

For normal SAXS experiments, the smearing effect due to the sample thickness is really small. A recently published paper demonstrated that the structural parameters calculated from the smeared data sets have little deviation from the ideal ones, which indicates that SAXS data collected in pink-beam mode can be used directly for structural calculations and model reconstructions without a desmearing procedure [17]. Beyond these two factors, the instrument configuration (the profile and divergence of incident beam) and the detector position sensing inaccuracies play a major role in the smearing of the detected scattering pattern. Most SAXS instruments are designed for optimum resolution in reciprocal space and thus the beam is usually focused onto the detector to minimize the smearing effect due to beam size

and divergence. For micro-beam applications, however, the focus lies preferentially at the sample position, and a compromise has to be found between a minimum beam size and an optimum SAXS resolution. According to Eq. (3), the μSAXS resolution can be estimated by assuming Gaussian functions for the beam profile at the detector as well as for the detector point spread function. Taking into account that the beam size (3.5 mm×1.1 mm at the detector position) as shown in Fig. 3(c) is much larger than the detector point spread function (80 μm for the Mar165), the FWHM width of the (Gaussian) resolution function can be approximated by the beam size at the detector plane. Furthermore, we calculated the μSAXS resolution at an energy of 10 keV and scattering vector of q= 0.6 nm^{-1} based on Eq. (2, 3), giving a finite wavelength contribution σ_λ =1.0×10^{-4} nm^{-1}, detector pixel size contribution $\sigma_{\rm D}$ =8.6×10^{-4} nm^{-1}, and finite collimation contribution $\sigma_{\rm D}$ =3.7×10^{-2} nm^{-1}(horizontal) and 1.2×10^{-2} nm^{-1}(vertical), so the total μSAXS resolution $\sigma_{\rm tot}$ =3.7×10^{-2} nm^{-1}(horizontal) and 1.2×10^{-2} nm^{-1}(vertical) is equal to the finite collimation resolution. Thus, the compound smearing contributions for μSAXS at BL16B1 can be directly evaluated as the image of the direct beam on the detector.

3.2 Desmearing procedure for two-dimensional μSAXS data

To analyze SAXS data measured with significant instrumental smearing, many desmearing methods have been developed. These mainly use iterative desmearing procedures, such as the Lake algorithm (for 1D SAXS patterns) and the Van Cittert method [16]. In general, these methods are not easy to handle. Besides, using these algorithms for desmearing a large number of data sets are inconvenient and can be time-consuming. 2D desmearing of centrosymmetric SAXS patterns has been developed using the Wiener filtering method, but the limitations of applying this filter make it a tedious task [18].

In computer vision and image processing, image restoration has been a research focus because of the degradation of image resolution and contrast, as shown in Fig. 4. Existing image restoration algorithms, such as inverse filtering, Wiener filtering and the Lucy-Richardson algorithm, build on known PSFs. However, in practice the PSF is often unknown or uncertain because of the complexity of imaging conditions. As shown in Fig. 3(d), the direct beam profile was recorded by a detector with an aluminum attenuator, so the PSF for the smeared μSAXS data is still uncertain. If used naively, the direct beam profile can lead to invalid restoration by classical restoration methods such as Wiener filtering. Therefore, application of blind deconvolution and restoration of the μSAXS data is necessary with uncertain PSFs in real experiments. Here, we present a robust and easy-to-use method to desmear 2D SAXS data. The blind deconvolution process can be completed by calling the "deconvblind" function in MATLAB, which is similar to the process of the damped Lucy-Richardson algorithm by accelerated convergence [19]. The Lucy-Richardson deconvolution algorithm is one of the most commonly used procedures for image deblurring/enhancement [20]. The algorithm works by calculating the maximum-likelihood solution for recovering an undistorted image that has been blurred by a known PSF. The undistorted image can be resolved via an iterative process using the following formula

$$I_{\rm resotre(}_{m+1}{\rm)}(x,y) = I_{\rm restore(}_{m}{\rm)}(x,y) \times \left[I_{\rm obs}(-x,-y) \otimes \frac{PSF(x,y)}{I_{\rm obs}(-x,-y) \otimes I_{\rm restore(}_{m}{\rm)}(x,y)} \right], \quad (4)$$

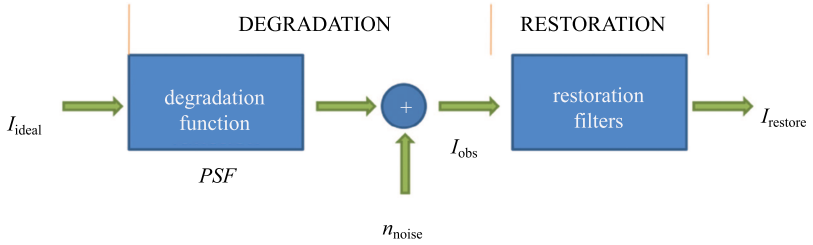

Fig. 4. A model of the image degradation and restoration process.

where $I_{\rm restore(m)}(x,\ y)$ is the estimate of the undistorted image in the mth iteration and "⊗" indicates the convolution operation. By using the "deconvblind" function in MATLAB, the restoration of the μSAXS image $I_{\rm obs}$ (Fig. 3(a, b)) was calculated with the initial PSF (Fig. 3(d)). The restored image and estimated PSF are output after a short processing time. The deblurring results of the μ SAXS defocus image (Fig. 5(b, c)) demonstrated high quality restoration when compared with the normal SAXS image (Fig. 5(a)).

In the process of deconvolution for Fig 3(a), a larger digital beamstop was needed for parastic scattering near

the beamstop, which may cause some deviation in the image restoration. The image blind restoration was accompanied by a ringing effect in the restored image, which was more obvious near the beamstop and the edge of the CCD. However, these deviations did not influence the analysis of the SAXS $I(q)$ fringe. As shown in Fig. 5(d, e), a fringe comparison was performed and showed good consistency between the restored image $I_{\rm restore}$ of the smeared image $I_{\rm obs}$ and the undesmeared normal SAXS image.

Due to the long, narrow beam profile on the CCD, the peak profiles were remarkably broadened in the horizontal direction, but were virtually invisible in the vertical direction. When the μSAXS data were desmeared, the $I(q)$ fringes were compared with the normal SAXS experimental results. The peak positions and widths of the $I(q)$ fringes are very important in SAXS data analysis, so the Gaussian function fitting results of the three peaks' positions and widths for bull collagen fibers are shown in Table 1, where $\Delta P/P = |P_{\rm obs} - P_{\rm normal}|/P_{\rm normal}$ and $\Delta W/W = |W_{\rm obs} - W_{\rm normal}|/W_{\rm normal}$ are the ratio of the peak and width deviation to the normal SAXS value. The peak position and width deviation in the vertical direction are hardly visible for small resolution functions according to Eq. (1), so the desmearing procedure was consequently unnecessary in the vertical direction. However, the effect of the desmearing procedure in the horizontal direction was very clear. The peak width deviations of processed images decreased to regular levels while the peak position deviations were still kept normal after treatment. Meanwhile, there were some deficiencies. Obviously, missing SAXS data in the low q zone can completely block Guinier analysis in the horizontal direction. This may be avoided by 90° rotation of the samples. All these results demonstrate the effectiveness and feasibility of this desmearing method. Finally, with this easy-to-use desmearing method, the μSAXS method at BL16B1 has become a complete system.

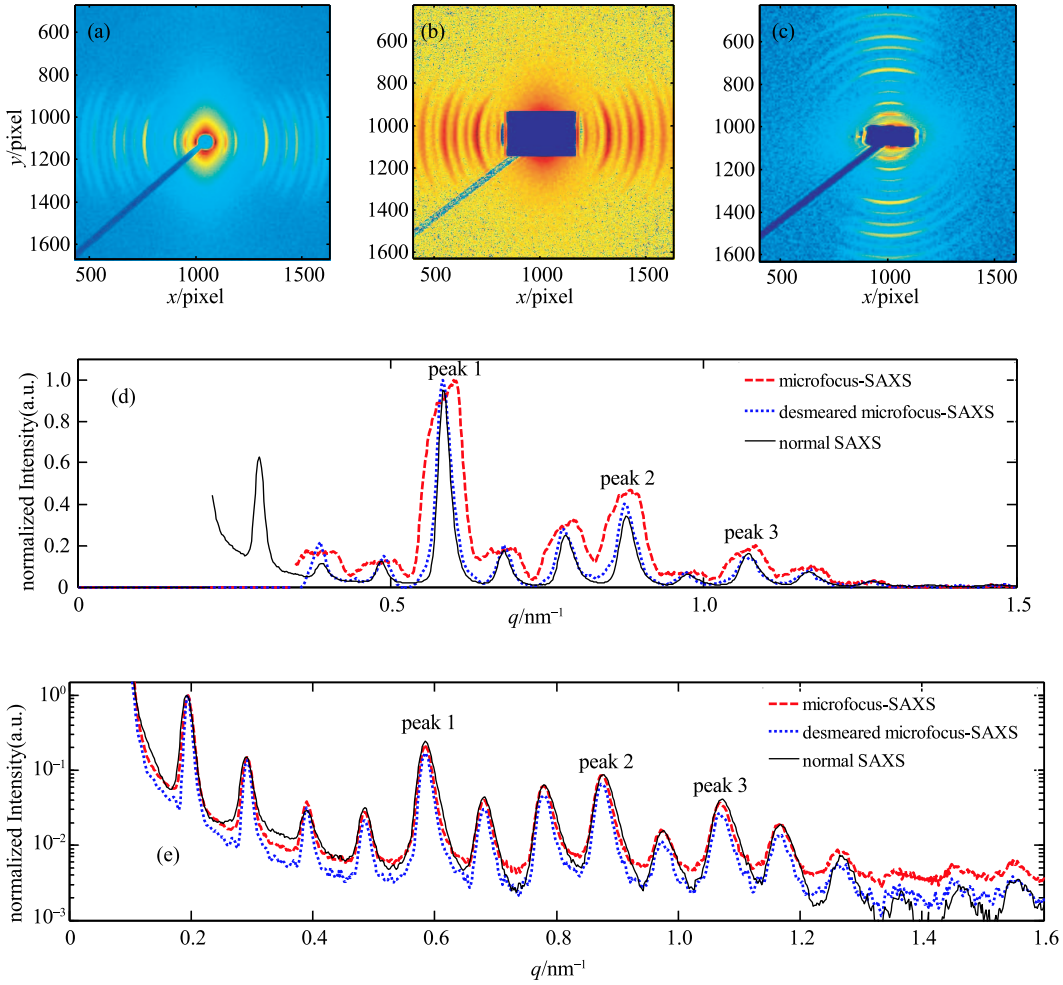

Fig. 5. (color online) (a) The normal SAXS image of horizontal placed bull collagen fiber; (b, c) the restored image for Fig. 3(a, b); (d, e) the $I(q)$ fringe comparison of Fig. 3 (a, b), Fig. 5(b, c) and 5(a).

Table 1. The fitting results of peak positions and widths as marked in Fig. 5(d, e) using Gaussian function.

		normal SAXS horizontal bull	μSAXS horizontal bull		μSAXS vertical bull	
			before desmeared	after desmeared	before desmeared	after desmeared
peak 1	P/nm^{-1}	0.5880	0.5871	0.5855	0.5853	0.5853
	$\Delta P/P$	-	0.15%	0.45%	0.46%	0.46%
	W/nm^{-1}	0.0232	0.0837	0.0283	0.0200	0.0176
	$\Delta W/W$	-	2.61	0.22	0.14	0.24
peak 2	P/nm^{-1}	0.8803	0.8760	0.8766	0.8755	0.8756
	$\Delta P/P$	-	0.49%	0.42%	0.55%	0.53%
	W/nm^{-1}	0.0290	0.0737	0.0345	0.0243	0.0223
	$\Delta W/W$	-	1.54	0.19	0.16	0.23
peak 3	P/nm^{-1}	1.0754	1.0725	1.0709	1.0704	1.0706
	$\Delta P/P$	-	0.18%	0.42%	0.46%	0.50%
	W/nm^{-1}	0.0325	0.0701	0.0368	0.0283	0.0270
	$\Delta W/W$	-	1.16	0.13	0.13	0.17

4 SAXS-CT for bamboo

To illustrate the performance of the μSAXS system at SSRF BL16B1, a bamboo sample was selected for the SAXS-CT experiment as shown in Fig. 6. The experiment was performed with 117 translations at a step size of 30 μm and 30 projection angles over 180°, with 20 s exposure time per frame. A total of 3510 SAXS patterns were collected in total 24 h. In Fig. 6(c) and (e), by selecting different integral regions of the scattering signals, different tomographic slices of the sample could be reconstructed. As shown in Fig. 6(a), a normal CT reconstruction for this bamboo sample was also performed at SSRF BL13W1, which could further verify the SAXS-CT results by overlapping Fig. 6(a) and (c) or (e). Furthermore, after reconstructing all the tomographic slices for each q, the 2D SAXS pattern at each location in the sample can be mapped. Fig. 6(g) shows the differences of the reconstructed 2D SAXS patterns for three different regions in the bamboo sample.

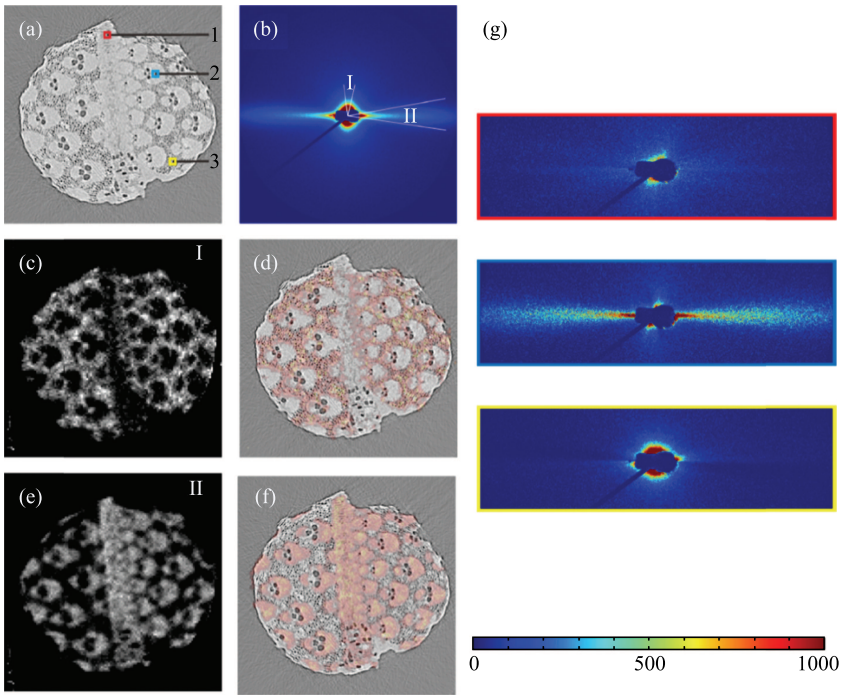

Fig. 6. (color online) SAXS-CT for the bamboo sample. (a) The X-ray absorption micro-CT slice of the bamboo sample (1: adhesive; 2: vascular bundle; 3: parenchyma cell). (b) Two-dimensional SAXS pattern of the bamboo sample. (c) Scattering tomographic slice reconstructed by integrating region I of (b). (d) Overlap between (c) and (a). (e) Scattering tomographic slice reconstructed by integrating region II of (b). (f) Overlap between (e) and (a). (g) Reconstructed 2D SAXS patterns for three locations in the bamboo sample, indicated by the red, blue and yellow squares.

5 Conclusion

To probe small scattering volumes, a μSAXS instrument has been established with a KB mirror system at SSRF BL16B1 and high-brilliance X-ray beams can be achieved on micrometer length scales. Two position-resolved scanning experimental methods (STXM and CT) were also developed for our users, which can be combined with μSAXS and μGISAXS methods. We have also reported an effective and easy-to-use desmearing procedure for two-dimensional SAXS pattern to improve the significant smearing effect in the horizontal direction. The application of this blind deconvolution procedure on the smeared SAXS pattern of a bull collagen fiber sample demonstrated the good restoration effect for the defocus blurred image in a short computation time. Furthermore, this desmeared procedure is also expected to be useful for data processing of tabletop SAXS and μSAXS. Finally, the SAXS-CT experimental results of a bamboo sample were presented to illustrate the performance of the μSAXS method. The long-term goal is to develop a user-friendly operation interface and proceed with online data analysis.

The authors would like to thank Dr. Xu-Ke Li for helpful discussions.

References

1 B. R. Pauw, J. Phys.: Condens. Matter, **26** (38): 239501 (2014)
2 T. Narayanan, *Synchrotron Small-Angle X-Ray Scattering*, (Berlin: Springer, 2008), p. 900
3 H. J. Xu, Z. T. Zhao, Nucl. Sci. Tech., **19** (1): 1–6 (2008)
4 F. Tian, X. H. Li, Y. Z. Wang et al, Nucl. Sci. Tech., **26**: 030101 (2015)
5 Z. H. Li, Z. H. Wu, G. Mo et al, Instrum. Sci. Technol., **42** (2): 128–141 (2014)
6 O. Paris, C. H. Li, S. Siegel et al, J. Appl. Crystallogr., **40**: s466–s470 (2006)
7 G. Q. Zheng, Z. Jia, X. Liu et al, Polym. Eng. Sci., **52** (4): 725–732 (2012)
8 L. Wang, W. Yang, S. He et al, Mater. Today Commun., **4** (11): 22–34 (2015)
9 O. Bunk, M. Bech, T. H. Jensen et al, New J. Phys., **11** (12): 123016 (2009)
10 T. H. Jensen, B. Martin, B. Oliver et al, Phys.Med. Biol., **56** (6): 1717–1726 (2011)
11 C. Riekel, M. Burghammer, R. Davies, IOP Conf. Ser. Mater. Sci. Eng., **14**: 012013 (2006)
12 A. Buffet, A. Rothkirch, R. Döhrmann et al, J. Synchrotron Rad., **19**: 647–653 (2012)
13 L. L. Zhang, S. Yan, S. Jiang et al, Nucl. Sci. Tech., **26**: 060101 (2015)
14 J. Bergenholtz, J. Ulama, M. Z. Oskolkova et al, J. Appl. Crystallogr., **49**: 47–54 (2016)
15 N. Stribeck, U. Nöchel. J. Appl. Crystallogr., **41**: 715–722 (2008)
16 T. Vad, W. F. C. Sager, J. Appl. Crystallogr., **44**: 32–42 (2011)
17 W. J. Wang, E. V. Shtykova, V. V. Volkov et al, J. Appl. Crystallogr., **48**: 1935–1942 (2015)
18 V. L. Flanchec, D. Gazeau, J. Taboury et al, J. Appl. Crystallogr., **29**: 110–117 (1996)
19 R. C. Gonzalez, R. E. Woods, B. R. Masters, J. Biomed. Opt., **14**: 331–333 (2009)
20 S. A. Hojjatoleslami, M. R. N. Avanaki, A. G. Podoleanu, Appl. Opt., **52** (23): 5663–5670 (2013)